PAN

Opto-Electronics Review

journal homepage: https://journals.pan.pl/opelre

Comparative study of reflectivity and pump scheme effects on the efficiency of Tm^{3+}-doped fibre laser at 1.72 µm

Mohamed Zaki[1]*, Mostafa Abouricha[1], Said Amrane[2],

[1] LPTHE, Department of Physics, Faculty of Sciences, Ibnou Zohr University, Agadir, Morocco
[2] STIC, Department of Physics, Faculty of Sciences, Chouaib Doukkali University, El Jadida, Morocco

Article info:

Article history:
Received 12 May 2024
Received in revised form 11 Aug. 2024
Accepted 23 Aug. 2024
Available on-line 27 Sep. 2024

Keywords:
thulium-doped fiber laser TDFL;
amplified spontaneous emission (ASE);
1.72 µm;
pump scheme.

Abstract

In this study, we revealed the impact of pumping scheme, fibre length, pumping power, and the reflectivity of the output fibre Bragg grating on the performance of a Tm^{3+}-doped fibre laser (TDFL) operating at a wavelength of 1.72 µm. Numerical simulations enabled the optimization of output power and the reduction of losses due to reabsorption, as well as amplified spontaneous emission (ASE) around 1820 nm. The Tm^{3+}-doped fibre (TDF) was bi-directionally pumped at 1570 nm to enhance pump absorption. The simulations suggest that a maximum power of 5.96 W at 1.72 µm and a slope efficiency of 64% are achievable using a Tm^{3+}-doped silica fibre with a bi-directional pump of 4 W forward and 6 W backward.

1. Introduction

Fibre laser sources emitting at wavelengths around 1700 nm, characterised by their high power, have attracted increasing interest due to their potential applications, notably in optical coherence tomography [1–3], laser surgery [4], remote sensing [5, 6], as well as for methane detection and in the processing of polymeric materials [7–9].

Many laser sources operating at a 1.72 µm wavelength have been developed recently, utilizing nonlinear optical frequency conversion methods, including optical parametric oscillators, and stimulated Raman scattering [10–13]. However, significant advances have been made through the use of rare-earth-doped fibres, offering a simpler and more robust solution for generating lasers at this wavelength. For example, Tm^{3+}-doped fibre lasers (TDFL) operating at 1.72 µm, which utilize energy level transitions within doped fibers, offer a wide emission range from 1650 nm to 2100 nm. These lasers can be efficiently pumped by erbium (Er)-doped fibre lasers at 1570 nm or Er/Yb co-doped hybrid fibres [14]. Although the first TDFL at 1.72 µm was introduced back in 2004 [15], these high-performance sources represent a recent innovation. This progress has paved the way for the direct use of these high-power fibre lasers, operating at 1.72 µm, as pumping sources for dysprosium (Dy)-doped fibers, enabling the generation of lasers in the mid-infrared range from 3 to 5 µm [16–18].

In recent years, much laser research has focused on improving the output power and efficiency of TDFL at 1.7 µm. These improvements include the use of fundamental transverse mode fibre laser pump sources from 1.55 to 1.6 µm, as well as careful design of the cavity layout [19,20]. An interesting approach was proposed by Zhang *et al*., who developed an intra-cavity pumping scheme by placing a 1.7 µm Tm^{3+}-doped fibre (TDF) cavity inside a 1560 nm Er/Yb-doped fibre cavity. This configuration aims to improve pump absorption and minimize reabsorption loss [14]. In addition, Zhang *et al*. used a 1720 nm Tm^{3+}-doped silica fibre cavity, pumped from both ends by two Er/Yb-doped cavity fibre lasers [21].

In this article, we conduct a comprehensive study of the output characteristics of a continuous-wave (CW) TDFL emitting at 1720 nm, which is powered by bidirectional pumping using two 1570 nm sources. The experimental setup, as demonstrated by Zhang *et al*. [21], is described, and a theoretical model based on the rate equations for the TDF is developed. The study then focuses on the impact of the distribution of pump power between the two ends of the fibre and the influence of the reflectivity of the output fibre Bragg grating (FBG) on the output power, the laser threshold, and the optimal length of the active fibre. The analysis of the results is carried out through numerical simulations.

*e-mail: mohamed.zaki@edu.uiz.ac.ma

https://doi.org/10.24425/opelre.2024.151988
1896-3757/ Association of Polish Electrical Engineers (SEP) and Polish Academic of Sciences (PAS). Published by PAS

2. Theoretical model

2.1. Fibre laser schematic

A schematic diagram of the 1720 nm TDFL is shown in Fig. 1. The device consists of two 1570 nm Er/Yb-doped fibre lasers, designated as pump sources [pump(+) forward and pump(-) backward], to enhance the injected pumping power. Additionally, a segment of commercial fibre (Nufern SM-TSF-9/125) was used as active fibre (TDF) with a low doping concentration $N_{Tm^{3+}} = 1.37 \cdot 10^{25}\ m^{-3}$ is surrounded by two FBGs, the first FBG_1, located at the entrance to the laser cavity, has a reflectivity $R_{s1} > 99.5\%$ at 1720 nm and a 3 dB bandwidth of 0.8 nm, the second FBG_2, positioned at the cavity exit with a reflectivity $R_{s2} = 45\%$ at 1720 nm and a 3 dB bandwidth of 0.2 nm. The pump(-) source directs a 1570 nm laser into the cavity using an isolator and a 1570/1720 nm wavelength multiplexer (WDM), which serves to separate the residual 1570 nm pump from the 1720 nm emitted laser. An optical circulator, functioning as an isolator, was installed between pump(+) and FBG_1 to prevent the return of the residual pump laser. In addition, the free port (port 3) of the circulator is initially designed for managing the reverse amplified spontaneous emission (ASE).

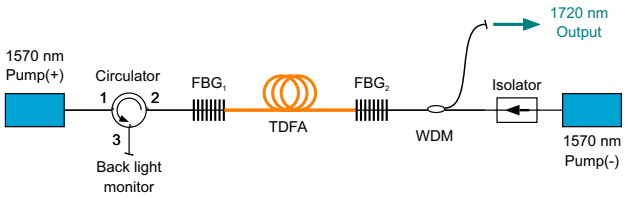

Fig. 1. The schematic of the 1720 nm TDFL.

2.2. Rate equations

To find the numerical solutions of a Tm^{3+}-doped silica fibre amplifier subjected to pumping in a broadband transition $^3H_6 \rightarrow ^3F_4$ that we have used here (see for example [22–24]), a model and method are verified in different fibre laser regimes (TDF [21] and Yb-doped fibre [25,26]) and are based on the traditional rate equations that have been described in detail in Refs. [27] and [28] and solved in the steady state considering the CW laser (i.e. time derivatives $\frac{dN}{dt} = 0$). The pump power, signal, and ASE propagation equations along the active fibre can be formulated as follows [21,29]:

$$\frac{dP_p^{\pm}(z)}{dz} = \pm P_p^{\pm}(z)\left\{\gamma_p\left[\sigma_e(\lambda_p)N_2(z) - \sigma_a(\lambda_p)N_1(z)\right] - \alpha_p\right\}, \quad (1)$$

$$\frac{dP_s^{\pm}(z)}{dz} = \pm P_s^{\pm}(z)\left\{\gamma_s\left[\sigma_e(\lambda_s)N_2(z) - \sigma_a(\lambda_s)N_1(z)\right] - \alpha_s\right\}, \quad (2)$$

$$\frac{dP_{ASE_i}^{\pm}(z)}{dz} = \pm P_{ASE_i}^{\pm}(z)\left\{\gamma_s\left[\sigma_e(\lambda_i)N_2(z) - \sigma_a(\lambda_i)N_1(z)\right] - \alpha_s\right\} + 2\sigma_e(\lambda_i)N_2(z)\frac{hc^2}{\lambda_i^3}\Delta\lambda, \quad (3)$$

where P^+_{p,s,ASE_i} and P^-_{p,s,ASE_i} represent the pump power, that of the signal laser and ASE signal at wavelength λ_i propagating along the z-axis forward and backward, respectively. In this model, the broadband ASE spectrum (1650–2100 nm) has been divided into $N_c \approx 400$ channels with a wavelength interval $\Delta\lambda$ of 1.12 nm. λ_i is the wavelength of the i^{th} channel, and ASE_i is the ASE power at wavelength λ_i. γ_p is the pump overlap factor estimated as the ratio of the core area to the cladding area, while γ_s is the laser signal overlap factor in the TDF. The propagation loss coefficients at the pump and signal wavelengths, denoted α_p and α_s, account for background and scattering losses in the TDF. The Tm^{3+} emission and absorption cross-sections, $\sigma_{ei} = \sigma_e(\lambda_i)$ and $\sigma_{ai} = \sigma_a(\lambda_i)$ are taken from Refs. [27] and [30], in particular $\sigma_a(\lambda_p)$, $\sigma_e(\lambda_p)$, $\sigma_a(\lambda_s)$, and $\sigma_e(\lambda_s)$ correspond to the pump and signal absorption and emission cross-sections. $N_1(z)$ and $N_2(z)$ describe the population densities of ions in the ground state $^3H_6$ and the upper state $^3F_4$ in the longitudinal position z of the fibre, respectively. $N_1(z)$ and $N_2(z)$ are linked by the following two relationships [26,31]:

$$\frac{N_2(z)}{N_{Tm^{3+}}} = \frac{\frac{\gamma_p\lambda_p\sigma_{ap}}{hcA_c}P_p(z) + \frac{\gamma_s}{hcA_c}\sum_{i=1}^{N_c}P(z,\lambda_i)\lambda_i\sigma_{ai}}{\frac{\gamma_p\lambda_p(\sigma_{ap}+\sigma_{ep})}{hcA_c}P_p(z) + \frac{\gamma_s}{hcA_c}\sum_{i=1}^{N_c}P(z,\lambda_i)\lambda_i(\sigma_{ai}+\sigma_{ei}) + \frac{1}{\tau}} \quad (4)$$

$$N_{Tm^{3+}} = N_1(z) + N_2(z), \quad (5)$$

where $P(z,\lambda_i) = P^{\pm}_{ASE_i}(z) + P^{\pm}_s(z)$ and $P_p(z) = P^+_p(z) + P^-_p(z)$, N_{Tm^3+} is the total population density of Tm^{3+} ions, τ is the spontaneous emission lifetime and $A_c = \pi \cdot r_c^2$ is the effective doping cross-section area with r_c which is the radius of the dope core. The numerical solution of (1)–(5) using the fourth-order Runge-Kutta method, introducing the boundary conditions specified in (6) and (7) for the pump and the laser signal, allows us to simulate the effect of the pumping configuration and the reflectivity on the performance of the TDFLs, such as the slope efficiency and the output power defined in (8).

$$P_p^+(0) = P_{p0}^+ \quad ; \quad P_p^-(L) = P_{pL}^- \quad (6)$$

$$P_s^+(0) = R_{s1}P_s^-(0) \quad ; \quad P_s^-(L) = R_{s2}P_s^+(L) \quad (7)$$

$$P_{out} = T_{s2}P_s^+(L).\delta, \quad (8)$$

where P^+_{p0} and P^-_{pL} are the pump powers launched into the front end (z = 0) by pump(+) source and the rear end (z = L) by pump(-) source , respectively; L is the length of TDF; R_{s1} and R_{s2} denote the reflectivity coefficient of the FBG_1 and FBG_2, respectively. P_{out} denotes the output power, T_{s2}

Table 1
Values of numerical parameters [29].

Quantity, Symbol	Value
Pump wavelength, λ_p	1570 nm
Signal wavelength, λ_s	1720 nm
Absorption cross-section at λ_p, σ_{ap}	$2.50 \cdot 10^{-25}$ m^2
Absorption cross-section at λ_s, σ_{as}	$3.13 \cdot 10^{-25}$ m^2
Emission cross-section at λ_p, σ_{ep}	$0.20 \cdot 10^{-25}$ m^2
Emission cross-section at λ_s, σ_{es}	$3.47 \cdot 10^{-25}$ m^2
Propagation loss at λ_p, α_p	$2.50 \cdot 10^{-2}$ m^{-1}
Propagation loss at λ_s, α_s	$2.00 \cdot 10^{-2}$ m^{-1}
Pump overlap factor, γ_p	0.70
Signal overlap factor, γ_s	0.70
Thulium concentration, $N_{Tm^{3+}}$	$1.37 \cdot 10^{25}$ m^{-3}
Core diameter, d_c	9 μm
Clad diameter	125 μm
Lifetime of the $^3F_4$ level, τ	0.25 ms
The insertion loss, δ	0.92

is the FBG$_2$ transmission coefficient such that $T_{s2} = 1 - R_{s2}$; δ indicates the insertion loss of the WDM at 1720 nm and the output optical isolator. The paraments of the TDF are summarized in Table 1.

3. Results and discussion

3.1. The effect of pumping scheme

We first study the influence of pumping scheme on amplifier output power, setting the total input pump power at 10 W. Figure 2 shows the evolution of output power as a function of fibre length for various pumping schemes (forward, backward, bidirectional). It can be seen that the bidirectional pumping scheme produces significantly higher output power at the optimum fibre length of 2.5 m.

When the active fibre length exceeded the optimum value, the output power at 1720 nm began to drop rapidly with increasing active fibre length in all three pumping configurations, due to greater cavity loss induced by signal reabsorption.

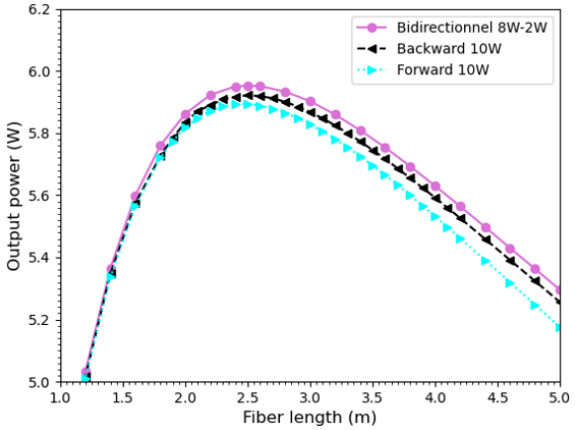

Fig. 2. Variation of output power calculated with the TDF length under different pumping configurations (forward, backward, and bidirectional).

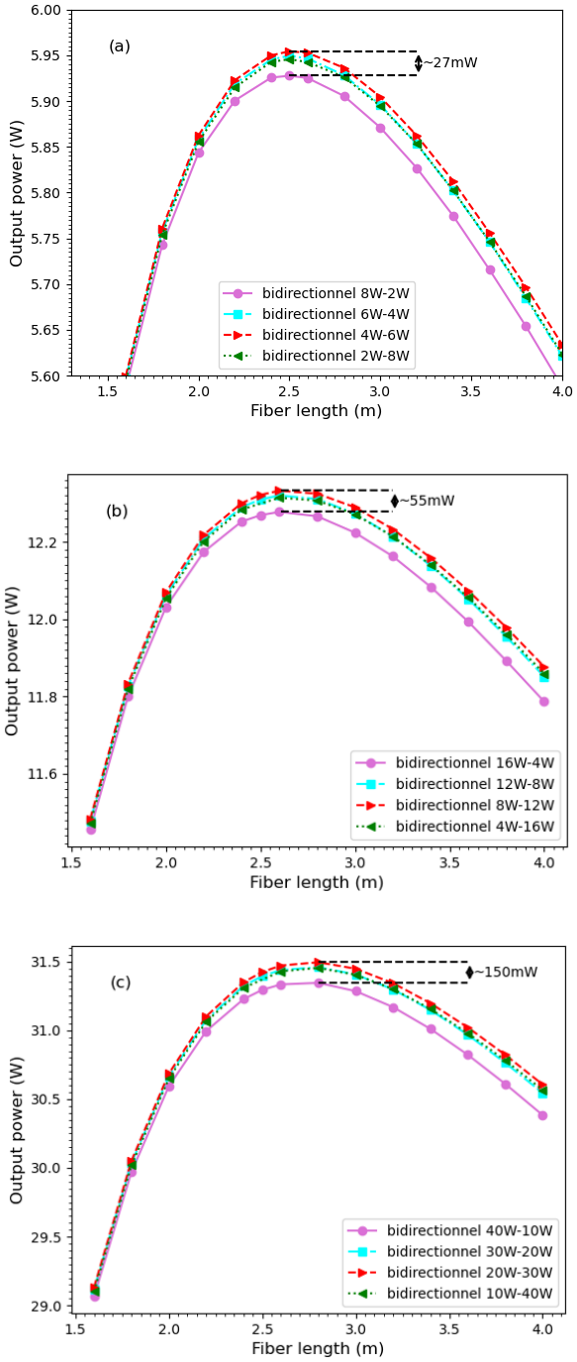

Fig. 3. Variation of output power calculated with the TDF length under different percentages of pump power launched in the case of the bidirectional pumping configuration. a) with 10 W of total pump power, b) with 20 W of total pump power, c) with 50 W of total pump power.

Next, we used the bidirectional pumping scheme, varying the percentage of total pumping power in both ends of the fibre to search for optimal values of pump(+) source pumping power $P_p^+(0)$ and pump(−) source pumping power $P_p^-(L)$ while keeping the total power value constant ($P_p^+(0) + P_p^-(L) = 10$ W) as shown in Fig. 3(a).

This analysis shows that when switching from the bidirectional pumping scheme (8 W–2 W), i.e., $P_p^+(0) = 8$ W from pump(+) source and $P_p^-(L) = 2$ W from pump(−) source to another scheme (4 W–6 W), the maximum output power at length of 2.5 m shows a minor increase of ≈ 27 mW

(+0.46%). This increase becomes more significant close to ≈ 55 mW when the total pump power is equal to 20 W and ≈ 150 mW(+0.48%) when the total pump power is equal to 50 W, as shown by Fig. 3(b) and Fig. 3(c) where pump powers of 20 W and 50 W are used, respectively.

Figure 4 illustrates the relationship between the 1720 nm output power and the 1570 nm pump power for a 2.5 m TDF. A variation in the threshold pump power is observed, shifting from 0.7 W in an (8 W–2 W) bidirectional pumping configuration with an efficiency of 63.1%, to 0.6 W in a (4 W–6 W) bidirectional pumping configuration, which shows a slightly higher efficiency of 63.7%. This means that the (4 W–6 W) bidirectional pumping scheme compares favorably with other bidirectional pumping configurations, delivering considerably higher output power at the optimum fiber length.

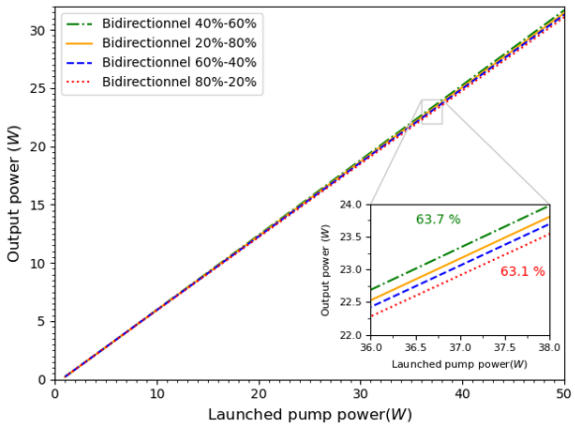

Fig. 4. Output power calculated at 1720 nm as a function of the lunched pump power at 1570 nm (with zoom in the inset).

As the total pump power increases, the optimal length of the active fibre is not constant at 2.5 m and changes in a monotone fashion, as indicated by figures Fig. 3(a), Fig. 3(b), and Fig. 3(c), and more specifically Fig. 5(a). The increase in optimal length is caused by the low pump reabsorption and the rise in ASE around 1820 nm. When the fibre length exceeds this optimal point, both the output power and efficiency significantly decrease due to the inability to suppress the ASE around 1820 nm. Furthermore, the improvement of the signal-to-noise ratio (SNR) is modest when transitioning from a signal at 1720 nm with a pump power of 10 W (≈ 53 dB) to a signal with a pump power of 50 W (≈ 56 dB), as indicated in Fig. 5(b). Consequently, selecting a pump power of 10 W is deemed suitable to circumvent temperature-related effects.

3.2. *The effect of reflectivity*

This section focuses on studying the influence of the reflectivity of the output Bragg grating (FBG_2) on the output performance under different pump schemes, with the launched pump power set at 10 W. According to the results illustrated in Fig. 6(a), it is noted that the output power at a wavelength of 1720 nm decreases with an increase in the reflectivity of the FBG. This trend is explained by a limitation in the power extraction rate within the laser cavity. In a bidirectional pumping configuration (4 W-6 W), the effect

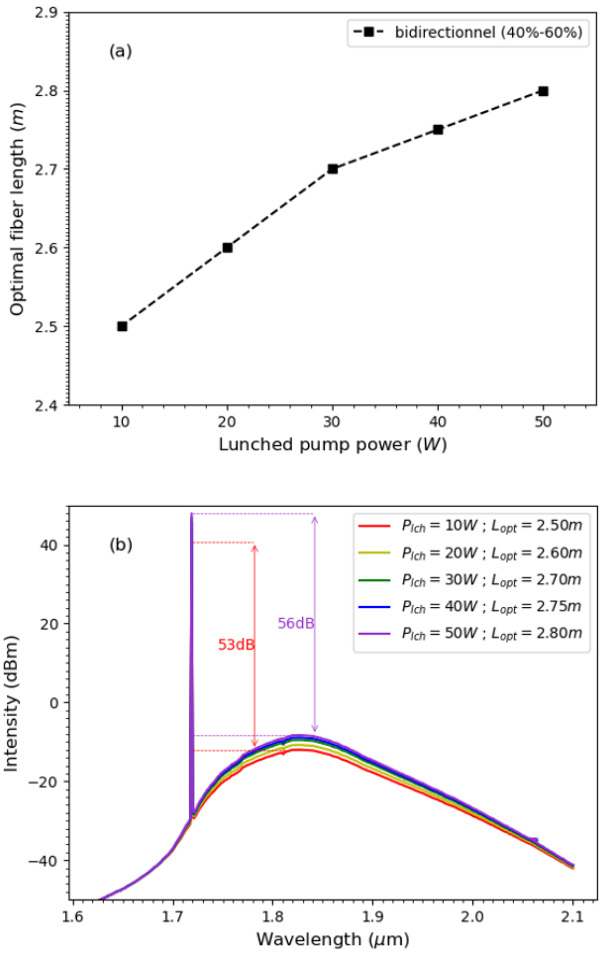

Fig. 5. (a) Optimal length of TDF as a function of applied pump power and (b) calculated laser spectrum at various pump powers, utilizing the most suitable TDF length for each selected lanched pump power.

of reflectivity on output power is more pronounced, likely due to the increased intensity of the light reflected back towards the source.

On the other hand, using an output FBG with low reflectivity reduces the intra-cavity signal power, which limits the ability to efficiently extract the gain from the TDF. In this case, the spectral width of the ASE broadens, and its intensity at 1850 nm strengthens, directly influencing the performance of the laser at 1720 nm in terms of the SNR as demonstrated in Fig. 6(b). Consequently, to optimize the output power of the laser at 1720 nm, it would be preferable to choose an output FBG with a moderate reflectivity like R_{s2} = 45%, which has already been used in previous simulations.

4. Conclusions

To conclude, this detailed numerical study examines the output characteristics of a thulium-doped silica fibre laser emitting at a wavelength of 1720 nm, based on a bidirectional pumping configuration. The analysis focused on the impact of several parameters, including pump power at 1570 nm, the length of the TDF, and the reflectivity of the output FBGs. The results reveal a maximum output power of 5.96 W, a slope efficiency of 64%, and a reduced laser

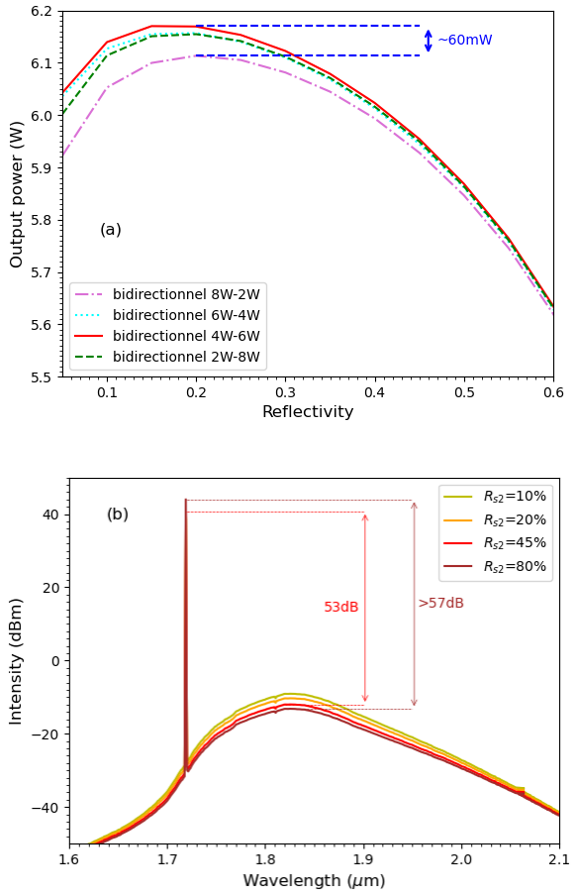

Fig. 6. a) Variation of output power with the reflectivity of the output FBG_2 for a 2.5 m TDF under different pumping configurations. b) Calculated laser spectrum at various reflectivities of the output FBG_2, using the optimal bidirectional pumping configuration (4 W–6 W).

threshold to 0.6 W, achieved with a 2.5 m TDF in a bidirectional pumping setup (4 W forward and 6 W backward). We anticipate that these findings will contribute significantly to enhancing the performance of TDFL, particularly around the 1720 nm wavelength.

References

[1] Sharma, U., Chang, E. W. & Yun, S. H. Long-wavelength optical coherence tomography at 1.7 µm for enhanced imaging depth. *Opt. Express* **16**, 19712–19723 (2008). https://doi.org/10.1364/OE.16.019712.

[2] Yamanaka, M., Teranishi, T., Kawagoe, H. & Nishizawa, N. Optical coherence microscopy in 1700 nm spectral band for high-resolution label-free deep-tissue imaging. *Proc. SPIE.* **10053**, 100631X (2017). https://doi.org/10.1117/12.2254772.

[3] Chong, S. P. *et al.* Noninvasive, in vivo imaging of subcortical mouse brain regions with 1.7 µm optical coherence tomography. *Opt. Lett.* **40**, 4911–4914 (2015). https://doi.org/10.1364/OL.40.004911.

[4] Wu, M., Jansen, K., van der Steen, A. F. & van Soest, G. Specific imaging of atherosclerotic plaque lipids with two-wavelength intravascular photoacoustics. *Biomed. Opt. Express* **6**, 3276–3286 (2015). https://doi.org/10.1364/BOE.6.003276.

[5] Schowengerdt, R. A. *Remote Sensing: Models and Methods for Image Processing.* (Elsevier, 2006).

[6] Emami, S. D., Dashtabi, M. M., Lee, H. J., Arabanian, A. S. & Rashid, H. A. A. 1700 nm and 1800 nm band tunable thulium doped mode-locked fiber lasers. *Sci. Rep.* **7**, 12747 (2017). https://doi.org/10.1038/s41598-017-13200-x.

[7] Mingareev, I. *et al.* Welding of polymers using a 2 µm thulium fiber laser. *Opt. Laser Technol.* **44**, 2095–2099 (2012). https://doi.org/10.1016/j.optlastec.2012.03.020.

[8] Anselmo, C., Welschinger, J.-Y., Cariou, J.-P., Miffre, A. & Rairoux, P. Gas concentration measurement by optical similitude absorption spectroscopy: methodology and experimental demonstration. *Opt. Express* **24**, 12588–12599 (2016). https://doi.org/10.1364/OE.24.012588.

[9] Chambers, P., Austin, E. A. & Dakin, J. P. Theoretical analysis of a methane gas detection system, using the complementary source modulation method of correlation spectroscopy. *Meas. Sci. Technol.* **15**, 1629 (2004). https://doi.org/10.1088/0957-0233/15/8/034.

[10] Dong, J. *et al.* High order cascaded raman random fiber laser with high spectral purity. *Opt. Express* **26**, 5275–5280 (2018). https://doi.org/10.1364/OE.26.005275.

[11] Ma, R., Quan, X., Zhao, T., Fan, D. Y. & Liu, J. Robust 1.69 µm random fiber laser with high spectral purity based on ordinary fibers. *J. Light. Technol.* **40**, 3942–3946 (2022). https://opg.optica.org/jlt/abstract.cfm?URI=jlt-40-12-3942.

[12] Zhang, Y. *et al.* Tunable random raman fiber laser at 1.7 µm region with high spectral purity. *Opt. Express* **27**, 28800–28807 (2019). https://doi.org/10.1364/OE.27.028800.

[13] Pei, W., Li, H., Huang, W., Wang, M. & Wang, Z. Pulsed fiber laser oscillator at 1.7 µm by stimulated raman scattering in h 2-filled hollow-core photonic crystal fibers. *Opt. Express* **29**, 33915–33925 (2021). https://doi.org/10.1364/OE.440461.

[14] Zhang, L. *et al.* 1.7- µm tm-doped fiber laser intracavity-pumped by an erbium/ytterbium-codoped fiber laser. *Opt. Express* **29**, 25280–25289 (2021). https://doi.org/10.1364/OE.432898.

[15] Agger, S., Povlsen, J. H. & Varming, P. Single-frequency thulium-doped distributed-feedback fiber laser. *Opt. Lett.* **29**, 1503–1505 (2004). https://doi.org/10.1364/OL.29.001503.

[16] Majewski, M. R. *et al.* Emission beyond 4 µm and mid-infrared lasing in a dysprosium-doped indium fluoride (inf 3) fiber. *Opt. Lett.* **43**, 1926–1929 (2018). https://doi.org/10.1364/OL.43.001926.

[17] Majewski, M. R., Woodward, R. I. & Jackson, S. D. Dysprosium mid-infrared lasers: current status and future prospects. *Laser Photonics Rev.* **14**, 1900195 (2020). https://doi.org/10.1002/lpor.201900195.

[18] Tang, Z. *et al.* Study of mid-infrared laser action in chalcogenide rare earth doped glass with dy 3+, pr 3+ and tb 3+. *Opt. Mater. Express* **2**, 1632–1640 (2012). https://doi.org/10.1364/OME.2.001632.

[19] Burns, M. D. *et al.* 47 w continuous-wave 1726 nm thulium fiber laser core-pumped by an erbium fiber laser. *Opt. Lett.* **44**, 5230–5233 (2019). https://doi.org/10.1364/OL.44.005230.

[20] Daniel, J., Simakov, N., Tokurakawa, M., Ibsen, M. & Clarkson, W. Ultra-short wavelength operation of a thulium fibre laser in the 1660–1750 nm wavelength band. *Opt. Express* **23**, 18269–18276 (2015). https://doi.org/10.1364/OE.23.018269.

[21] Zhang, L. *et al.* High-efficiency thulium-doped fiber laser at 1.7 µm. *Opt. Laser Technol.* **152**, 108180 (2022). https://doi.org/10.1016/j.optlastec.2022.108180.

[22] Khamis, M. & Ennser, K. Enhancement on the generation of amplified spontaneous emission in thulium-doped silica fiber at 2 µm. *Opt. Commun.* **403**, 127–132 (2017). https://doi.org/10.1016/j.optcom.2017.07.032.

[23] Romano, C., Tench, R. E. & Delavaux, J.-M. Simulation of 2 µm single clad thulium-doped silica fiber amplifiers by characterization of the 3 f 4–3 h 6 transition. *Opt. Express* **26**, 26080–26092 (2018). https://doi.org/10.1364/OE.26.026080.

[24] Jackson, S. D. Towards high-power mid-infrared emission from a fibre laser. *Nat. Photonics* **6**, 423–431 (2012). https://doi.org/10.1038/nphoton.2012.149.

[25] Shang, L. Comparative study of the output characteristics of ytterbium-doped double-clad fiber lasers with different pump schemes. *Optik* **122**, 1899–1902 (2011). https://doi.org/10.1016/j.ijleo.2010.11.021.

[26] Ren, Y., Cao, J., Du, S. & Chen, J. Numerical study on the continuous-wave yb-doped fiber amplifiers operating near 980 nm. *Optik* **161**, 118–128 (2018). https://doi.org/10.1016/j.ijleo.2018.02.006.

[27] Peterka, P., Faure, B., Blanc, W., Karasek, M. & Dussardier, B. Theoretical modelling of s-band thulium-doped silica fibre amplifiers. *Opt. Quantum Electron.* **36**, 201–212 (2004). https://doi.org/10.1023/B:OQEL.0000015640.82309.7d.

[28] Jackson, S. D. & King, T. A. Theoretical modeling of tm-doped silica fiber lasers. *J. Light. Technol.* **17**, 948 (1999). https://opg.optica.org/jlt/abstract.cfm?URI=jlt-17-5-948.

[29] Zhang, L. *et al.* Efficient multi-watt 1720 nm ring-cavity tm-doped fiber laser. *Opt. Express* **28**, 37910–37918 (2020). https://doi.org/10.1364/OE.411671.

[30] Peterka, P., Kasik, I., Dhar, A., Dussardier, B. & Blanc, W. Theoretical modeling of fiber laser at 810 nm based on thulium-doped silica fibers with enhanced 3 h 4 level lifetime. *Opt. Express* **19**, 2773–2781 (2011). https://doi.org/10.1364/OE.19.002773.

[31] Cheng, H., Lin, W., Zhang, Y., Jiang, M. & Luo, W. Numerical insights into the pulse instability in a ghz repetition-rate thulium-doped fiber laser. *J. Light. Technol.* **39**, 1464–1470 (2021). https://doi.org//10.1109/jlt.2020.3034397.